AIAA 2003-1069

High Efficiency Forward Swept Propellers at Low Speed

C. Paxton, P. Gryn, E. Hines, U. Perez, and G.-C. Zha
University of Miami
Coral Gables, FL

41st Aerospace Sciences Meeting & Exhibit
6–9 January 2003
Reno, Nevada

HIGH EFFICIENCY FORWARD SWEPT PROPELLERS AT LOW SPEED

Craig D. Paxton*, Peter J. Gryn†, Erisa K. Hines‡, Ulises Perez* and Ge-Cheng Zha§
Dept. of Mechanical Engineering
University of Miami
Coral Gables, FL 33124
Email: zha@apollo.eng.miami.edu

Abstract

Propellers with forward sweep were studied in order to determine whether this type of sweep produces a more efficient propulsion source. The sweep effect is achieved solely by tangentially leaning the leading edge of the blades toward the direction of rotation. Eight 155mm (6.1") diameter propeller designs were created for testing; one straight blade, used for comparison, and seven swept blades using different sweep angles and configurations. Wind tunnel tests were conducted on all blades and CFD simulations were made for the straight blade as well as the best performing swept designs from the wind tunnel results. While efficiency values from wind tunnel tests and CFD simulations were not the same, the trends created in both were considered to be comparable. The general trend established shows that the swept blades not only have higher efficiencies but also have greater stall margins. Some speculated reasons for these advantages are given.

1. Introduction

The vast majority of general aviation aircraft in the world are powered by propeller engines, which include subsonic military and civil transports, agriculture and emergency rescuer airplanes, private airplanes, UAV's, model airplanes, etc. Thus, improvement of propeller performance could potentially have a large impact by reducing fuel consumption and noise levels.

After War World II, the design of an aft swept wing achieved great success and is widely used for modern high subsonic, transonic, and supersonic airplanes. Inspired by the success of the aft swept wing, efforts were made in the 1940-50's to design aft swept propeller blades.[1] In the late 1970's and into the 1980's, under the background of the world oil crisis, interests were revived to conduct advanced propeller design. NASA made a series of designs and suggested tests for implementing aerodynamic sweep.[2,3,4,5,6] Significant improvements in efficiency and noise reduction were achieved at high subsonic Mach numbers (0.7-0.8).[6] NASA's work at that time focused primarily on single rotation propellers by using an axial backward aerodynamic sweep similar to that researched in the 1940-50's.[1,2,3,4,5,6]

To further explore the theoretically higher efficiency of a turboprop when compared to a turbofan, counter-rotating propeller concepts were proposed to reduce the swirl loss induced by a single propeller blade.[6] General Electric conducted a design of counter-rotating propellers as a contract from NASA in 1994.[7] The front propeller blades were designed using forward sweep to increase the space between the two propellers in order to reduce the propeller interaction and noise. However, the wind tunnel tests for the counter-rotating propellers failed due to the blade structure instability (flutter) and the research work was not continued.[8] So far, no results on forward tangential swept propeller blades have been reported for propellers.

After War World II, many efforts were made to employ backward aerodynamic sweep technology for an aircraft engine fan/compressor in order to improve efficiency and stall margin characteristics. No break through using any type of sweep was achieved until 1998 when GE Aircraft Engines announced they had succeeded in using forward sweep to improve the stall margin and efficiency of a two-stage fan.[9] The mechanisms that cause the forward swept blade to have a better performance are that the tip touches "clean air" first, pulls more mass flow, and has higher flow kinetic energy, which helps to suppress the tip vortex. The turbulence intensity in the tip-endwall boundary layer is

* Senior Undergraduate Student (current Graduate Student, University of Miami), AIAA Student Member
† Senior Undergraduate Student, AIAA Student Member
‡ Senior Undergraduate Student (current Graduate Student, MIT), AIAA Student Member
§ Associate Professor, AIAA Member

also likely to be lower and would therefore generate less noise.

The purpose of this paper is to explore the possible advantages of applying forward sweep to a single rotation aircraft propeller. It is natural to be inspired to apply the successful experience of forward sweep in the fan/compressor design to a propeller. The benefits of aerodynamic sweep for propellers seem most useful at reducing the effective Mach number in the high-speed region (i.e. Mach number = 0.7-0.8).[6] Due to the constraints of manufacturing and test facilities available to the present authors, research began with low speed forward swept propeller design and testing as the first step to study this technology. These propellers are designed to operate in the incompressible region with a maximum Mach number of 0.3 as shown in Figure 1. Further research on the forward swept propeller in the high-speed region as well as full-scale model testing is the next step.

The method for sweeping these propeller designs is different from historically attempted methods. In the past, sweep was mostly in the axial direction, similar to the backward sweep used for airframe wing design. The forward sweep discussed in this paper is entirely achieved by tangential sweep. In other words, when "forward sweep" is referred to, it means that the outer-span of the propeller blade is swept forward in the direction of rotation unless otherwise stated.

Three different sweep configurations were created during this research. The first forward swept design created has an inner span region that is intentionally designed as backward sweep followed by the outer-span region being swept forward. This configuration is similar to an arched bird wing, which has backward sweep near the bird body and forward sweep in the wing tip.[10] Actually, the flapping arched shape bird wings create the forward sweep effects at the tip in the same way as mentioned above for this forward swept propeller design. With the optimization in the nature's evolution, it is believed that there are some aerodynamic advantages in the way that birds fly. The second and third designs incorporate only forward sweep. One design has the inner-span region without any sweep and the other design incorporates forward sweep along the entire blade length. These designs were created to study the effect of different forward sweep distributions.

2. Aerodynamic Design

The propellers studied in this paper are two blade propellers with a diameter of 155mm. To have a basis for comparison, a straight blade was designed first. The straight blade was designed to mimic the performance of a Graupner 5.9"x5.9" CAM speed propeller, which has the ability to fly at a cruise velocity of 27 m/s (60 mph) at 12,100 RPM. The straight blade has the same chord and thickness values at identical radii as the Graupner blade.

In all, seven swept blades were designed; four blades with different angles of backward-forward sweep, one outer-span forward swept design, and two designs with completely forward sweep. As mentioned before, the sweep effect is achieved solely by tangentially leaning the leading edge toward the direction of rotation. The leading edge has a constant axial position across the entire blade span. Therefore, the sweep effect is created only by tangentially leaning the blade without use of axial sweep. An advantage of the tangential sweep is that it takes no extra axial space compared with the conventional radial blade.

Figures 2, 3, and 4 show a plane-of-rotation view for the backward-forward, outer-span forward, and completely forward leading edge sweep configurations, respectively. For all of the backward-forward sweep combinations the backward swept portion (opposite to the direction of rotation, ω) starts at the radius of the root, r_{root}, and continues till it has reached the vertical distance equal to 1/3 of the blade span (1/3 distance from r_{root} to r_{tip}, ξ) at the angle ϕ measured clockwise from the radial line (see Figure 2). The forward swept segment begins at the end of the backward sweep at the angle ψ measured counterclockwise from the radial line until it intersects the radius of the propeller tip, r_{tip}. A circle that is tangent to both lines, B, connects the backward and forward swept leading edge lines; this is referred to as the elbow region. The four backward-forward swept configurations made were 5-10, 10-15, 15-20, and 20-30, where the first number is the backward sweep angle and the second is the forward sweep angle. From this point forward, the backward-forward sweep blades will be referred to as 5-10, 10-15, 15-20, and 20-30. The radius for the tangent circle connecting the backward and forward swept portion is 80mm for 5-10, 50mm for 10-15, 35mm for the 15-20, and 25mm for the 20-30.

The outer-span forward swept blade differs by starting without a backward swept region. The leading edge starts from r_{root} with a straight radial direction until it reaches the ξ location where it then begins its forward sweep at the angle ψ until it intersects r_{tip} (see Figure 3). Only one outer-span forward swept configuration was constructed with a forward sweep angle of 15° and the same ξ location as that of the backward-forward

sweep configuration. From this point forward, the outer-span swept blade will be referred to as 00-15.

The completely forward swept configuration was constructed by extending the leading edge from r_{root} with a constant forward sweep angle ψ until it intersects r_{tip} (see Figure 4). Two completely forward swept configurations were constructed for testing, one with a 10° and the other with a 20° forward sweep angle. From this point forward, the completely forward swept configurations will be referred to as 10-Forward and 20-Forward, respectively.

The backward-forward swept blade shown in Figure 2 was designed to enhance the effect due to forward sweep, especially in the tip region, in order to suppress the tip vortex. The advantage of this design, from the structural point of view, is that the center of gravity is in the same tangential location as the straight blade, thus avoiding additional stresses on the root.

In both the outer-span and completely forward designs (see Figure 3 and 4), the constant sweep angle was used to study the effect of purely forward swept configurations. The disadvantage of the purely forward swept configurations is that the center of gravity is shifted forward off the radial line, thus increasing the stress at the root. However, no blades failed due to structural problems during wind tunnel tests.

All blades were designed so that the airfoils are exactly the same at identical radial locations. That is the airfoil shape, maximum thickness, chord length, stagger angle, and angle of attack are the same for the straight and swept blades at the same radius locations (i.e. point C and D have the same airfoil; point E and F have the same airfoil – as seen in Figures 2, 3, and 4). This was done to ensure that the performance difference observed between the straight and swept blades was due solely to the sweep effect. This dictates that the only difference among the blades is the sweep configurations. The straight blade can be seen as a special case where the sweep angle $\phi=\psi=0$.

To design a propeller, certain desired parameters such as blade diameter, cruise speed, and RPM must be selected to match an airplane's power requirements. The wind tunnel first used for testing is an Aerolab educational wind tunnel, located at the University of Florida which has a test section size of 305mm x 305mm x 457mm (12"x12"x18"). To reduce wall effect from the test section, the diameter was chosen to be 155mm (6.1"), which is approximately half the size of the test section. A cruise velocity of 27 m/s (60mph) and RPM of 12,100 were selected to match the commercial Graupner blade.

R.A.F.-6 and Clark Y are the most commonly used airfoils for propeller blades with the Clark Y being the preferred.[11] Results showed that the R.A.F.-6 airfoil fared better at climb and take-off for high-speed planes; however, the Clark Y produces higher peak efficiencies on low-pitch propellers with overall efficiency increasing as blade thickness increases. These findings are the reasons that the Clark Y airfoil was selected for the present design. Figure 5 shows the stacking of the Clark Y airfoil sections along the leading edge and Figure 6 shows the front view of the straight (left), 10-15 (middle), and 20-Forward (right) blades.

Figure 7 shows the relative angle of attack (based on the 2D inviscid model) distribution along the radius as it varies from low to high speeds for all propeller blades. The figure shows that at the speed of 27 m/s, the angle of attack is 3° along the entire radius of the blade; this is because the blade was designed to reach its optimum efficiency at that speed. Because the Clark Y and R.A.F.–6 airfoils are similar, the 3° angle of attack was determined to be optimal from an angle of attack vs. D/L (drag/lift) graph, Figure 8, for a R.A.F.–6 airfoil using a maximum thickness to chord ratio equivalent to 0.15.[11,12]

Manufacturing techniques were limited due to material selection and production cost. Two suitable techniques were made available through sponsorship from Stratasys Inc in Minneapolis, MN and Sermatech Castings in Miami, FL. Stratasys, a fused deposition modeling (FDM) company, provided FDM propellers for the straight, 10-15, 15-20, and 20-30 backward-forward sweep configuration propellers. The advantages of these polycarbonate propellers are the precision associated with the manufacturing method and the smooth finish on the final product. The disadvantages are the lack of rigidity and the lack of trailing edge definition.

Sermatech Castings provided aluminum sand castings that were cast from molds made around the 3D wax printouts of the Pro/E geometry. These aluminum castings provide a high rigidity, which helps hold the geometric twist during testing, and have a relatively smooth surface finish. However, due to complications with casting extremely thin geometry, the blades did lose definition on the trailing edge and some blades became twisted during the process. For these reasons, it is uncertain how precisely the aluminum propellers preserved the true aerodynamic shape. The blades that were chosen for wind tunnel tests appeared to adequately match the 3D wax printout prototypes.

3. Wind Tunnel Tests

3.1 Testing

Tests were conducted in the Aerolab educational wind tunnel at the University of Florida. The first tests were conducted on March 23 and 24, 2002. Due to manufacturing problems, the only aluminum blades prepared for the first tests were the straight and 15-20. In addition, they were only tested at 26, 28, and 30 m/s due to a concern that the motor's speed controller would overheat due to the additional weight of the aluminum blades. All polycarbonate blades were tested in the first tests; however, data yielded inconclusive results since the material's low rigidity allowed deflection during testing.

A second set of wind tunnel tests was conducted, on July 26 and 27, 2002, using only the aluminum blades in order to remove the uncertainty of material flexibility. The blades tested were the straight, 5-10, 10-15, 15-20, 20-30, 00-15, 10-Forward, and 20-Forward. Testing was conducted at the speeds of 8, 12, 16, 20, 24, 26, 28, 30, 32, and 34 m/s, which correspond to the advance ratios of 0.04, 0.06, 0.08, 0.10, 0.12, 0.13, 0.14, 0.15, 0.16, and 0.17, respectively. Because of restrictions caused by testing in a small wind tunnel, measurements were not taken below 8 m/s.

The wind tunnel used was a closed throat model with a cross section of 12"x12". To reduce interference of the boundary layer developed in the test section, the propellers were designed to have a diameter of approximately 6 inches.[13] Because of the changes in the static pressure inside a closed throat tunnel, a reaction occurs at the propeller causing a higher thrust to be produced at the assumed tunnel velocity than would normally be produced, thus a correction factor is necessary. The correlation:

$$\frac{V'}{V} = 1 - \frac{\tau_4 \alpha_1}{2\sqrt{1+2\tau_4}} \tag{3.1}$$

accounts for these effects and was applied to the data in order to negate any bias encountered.[13] In this equation, $\tau_4 = T/\rho A V^2$, $\alpha_1 = A/C$, V' is the corrected velocity [m/s], V is the freestream velocity [m/s], T is the thrust produced [N], ρ is the density of the fluid [kg/m^3], A is the propeller disk area [m^2], and C is the cross-sectional area of the tunnel test section [m^2].

The velocity in the test section was controlled by a closed loop feedback control system that regulated the tunnel speed to a specified constant velocity. Once the tunnel reached the desired speed, the RPM of the propeller motor was then adjusted to 12100 RPM using an optical tachometer, and the system was allowed to arrive at a steady-state condition before data was taken. Using a computer data acquisition system, the thrust produced by the propeller as well as the current and voltage supplied to the propeller motor was taken every second for 120 seconds. Statistical analysis of the data from both wind tunnel tests demonstrated that the data set was consistent.

3.2 Test Results

For all wind tunnel tests, the efficiency and advance ratio are defined as:

$$\eta = \frac{VT}{P} \tag{3.2}$$

and

$$J = \frac{V}{\omega D} \tag{3.3}$$

respectively. In these equations, V is the freestream velocity, T is the thrust produced by the propeller [N], P is the power used [Watts] (found by multiplying the voltage and current consumed by the propellers motor), ω is the angular velocity of the propeller [rad/s], and D is the diameter of the propeller [m]. Power losses due to the motor were assumed to be consistent for all blades tested.

Data from all tests performed on the aluminum blades was compiled and then plotted as efficiency vs. advance ratio as shown in Figure 9. For clarity, only the Graupner, straight, 00-15, 10-15, and 20-Forward blades are shown from the second test. The straight blade is displayed because it is the basis for comparing the swept designs. The 00-15, 10-15, and 20-Forward blades are shown because they had the largest peak efficiencies and stall margins of all the tested forward swept designs.

As seen in Figure 9, the results from the second test show that the 20-Forward propeller had higher efficiencies at most advance ratios as well as a larger stall margin (higher advanced ratio when efficiency reaches zero) than all other blades. The peak efficiency of the 15-20 blade is slightly higher than the 20-Forward; however, both forward swept blades have higher peak efficiencies and larger stall margins than the straight. It should be noted that the 00-15 blade has an increased stall margin similar to the 10-15 and 20-Forward blades, has a peak efficiency near that of the 20-Forward but at a lower advance ratio, and also has higher efficiencies at lower speeds similar to the straight blade. Also, all blades designed in this research have better efficiencies and stall margins than the commercial Graupner blade.

Coefficients of thrust and power are defined as:

$$C_T = \frac{T}{\rho \omega^2 D^4} \tag{3.4}$$

and

$$C_{power} = \frac{P}{\rho \omega^3 D^5} \tag{3.5}$$

respectively. In these equations ρ is the density [kg/m^3] and all other variables are as previously defined. These coefficients are plotted versus advance ratio in Figures 10 and 11 respectively, which together illustrate that the greater thrust produced by the swept blades overcomes the additional power consumed to achieve the higher efficiencies shown.

Figure 9 also shows a similar trend established in the first test, where the 15-20 blade outperforms the straight. However, the values from the first test are much higher than those of the second, which indicates that a problem was present in one of the two tests. It was also realized that a separate measurement should have been taken for the nacelle drag at each speed in order to find the total thrust produced by the propeller.[8] These results, however, can still be used as a preliminary guide since the blades will all be affected in the same manner. Further wind tunnel tests are planned to clarify this uncertainty.

4. CFD Simulation

4.1 CFD Setup

A computational fluid dynamics (CFD) simulation was carried out as an alternate means of studying the performance of the swept propeller blades. For this study, FLUENT was setup as a 3D segregated solver with implicit and absolute velocity formulations and a time-independent solution (steady). The inlet and far-field zones were set to the desired freestream velocity. Figure 12 shows the three-dimensional computational domain used to simulate the propeller flow in an open air field. This is different from the wind tunnel tests which were conducted in a confined space as described in the wind tunnel testing section. The CFD simulation is expected to exclude the wall boundary layer effects and result in higher efficiency values than the wind tunnel experiments. The purpose of the CFD simulations are to verify the trend of the wind tunnel tests, which indicated that the 10-15 and 20-Forward swept blades have higher efficiencies and larger stall margins than the straight blade.

The inlet boundary was placed 1000mm (approximately 13.5 blade lengths) in front of the origin and the outlet was placed 1000mm behind the origin. Due to the rotating reference frame, a far-field boundary was established at a constant radius of 1600mm (approximately 21.5 blade lengths) from the origin. These boundary conditions were placed far from the propeller in order to reduce interaction with the flow induced by the propeller. The nosecone of the motor and nacelle, shown in Figure 13, were also constructed as part of the CFD model. The nacelle was extended to the outlet in order to simplify the geometry and CFD boundary conditions.

The Tet/Hybrid meshing scheme was used to create the volume mesh, this gives a mesh primarily constructed of tetrahedral elements but can contain hexahedral, pyramidal, and wedge elements where appropriate. The final cell count for the straight, 10-15, and 20-Forward flow volumes were 1,664,084, 1,053,210, and 1,522,865 respectively. These cell counts near the blade surface are about the same. The cell size difference is mostly from the domain away from the blade surface, and hence the CFD results difference due to the mesh size is minimal. A typical mesh around the airfoil at a mid-span location is given in Figure 14. The use of size functions allowed the grid mesh to be adequately small near the propeller while at the same time producing larger cells near the far-field.

The inlet and far-field zones were assigned as velocity inlet boundary conditions which Fluent describes as a zone where "the total (or stagnation) properties of the flow are not fixed, so they will rise to whatever value is necessary to provide the prescribed velocity distribution."[14] The outlet was assigned an outflow boundary condition, which Fluent says "are used to model flow exits where the details of the flow velocity and pressure are not known prior to solution of the flow problem."[14] In other words, no parameters are specified at outflow boundaries; FLUENT extrapolates the required information from the interior. The no-slip boundary condition was used for all walls and the Periodic rotational boundary condition is used for the two horizontal periodic planes.

Figure 1 shows the incoming relative Mach number at different freestream velocities with a range generally lower than 0.3. Hence, the incompressible flow solver was used. At high freestream velocities, there is a small region on the outer-span suction surface where the maximum Mach number reaches about 0.47. However, the incompressible flow domain is dominant and the incompressible solver used is appropriate. The Reynolds number based on the average chord length is approximately 100,000; therefore, the laminar viscous model was used.

4.2 CFD Results and Discussion

The three blades, straight, 10-15, and 20-Forward were the only blades examined in CFD. The 10-15 and 20-Forward blades were the only swept blades picked for CFD because wind tunnel tests showed they had the highest efficiencies and largest stall margins for their respective types of sweep, while the straight blade was created for comparison purposes only.

Efficiency results from CFD calculations are shown in Figure 15 as a plot of efficiency vs. advance ratio. Efficiency and advance ratio for all CFD results were calculated using:

$$\eta = \frac{VT}{\tau\omega} \tag{5.1}$$

and

$$J = \frac{V}{\omega D} \tag{5.2}$$

respectively. Where V is the freestream velocity [m/s], T is the thrust [N], τ is the torque [N·m], ω is the angular velocity [radians/s], and D is the propeller diameter [m].

In Figure 15, the 20-Forward blade has the highest efficiency, the straight blade has the lowest efficiency, and the 10-15 lies between. While the efficiency values are different from the wind tunnel tests, the overall trend is similar.

The coefficient of thrust, C_T, and coefficient of power, C_{power}, were created and are shown in Figures 16 and 17 respectively. C_T and C_{power} were calculated using:

$$C_T = \frac{T}{\rho\omega^2 D^4} \tag{5.3}$$

and

$$C_{power} = \frac{\tau\omega}{\rho\omega^3 D^5} \tag{5.4}$$

respectively. Where ρ is the density [kg/m^3] and all other variables are as defined previously. Both the 10-15 and 20-Forward blades have greater coefficients of thrust and power than the straight blade over most advance ratios. Even though the coefficient of power is greater, the larger coefficient of thrust allows the efficiency of both blades to surpass the straight.

To study the surface loading, the pressure coefficient, C_p, along the airfoil at the same radial locations for all three blades were plotted. Two locations along the blades were selected, one near the root at 36% of the blade radius and the other in the tip region at 94%. Figures 18, 19, and 20 are C_p plots at 36% of the blade radius and Figures 21, 22, and 23 are C_p plots at 94% of the blade radius, for the freestream velocities of 16, 26, and 32 m/s respectively. All C_P graphs measure chord length starting from the leading edge. Within Fluent the C_p is defined as:

$$C_P = \frac{(p - p_\infty)}{\frac{1}{2}\rho_\infty v_\infty^{\,2}} \tag{5.5}$$

where p is the static pressure, p_∞, ρ_∞, and v_∞ are freestream pressure, density, and velocity, respectively, and are designated by the user.

From Figures 18-23, it can be seen that for all speeds the two forward swept blades, in particular the 20-Forward blade, have a larger angle of attack and hence a higher blade loading than the straight blades. This supports the greater C_T for the 20-Forward blade illustrated in Figure 16. This higher loading also suggests that the swept blades, especially the 20-Forward, affect the flow near the blade in a way that slows down the decreasing angle of attack as the freestream velocity increases. In other words, the swept propeller blades tend to maintain a favorable positive angle of attack over a wider range of freestream velocities than the straight blade.

Figures 24, 25, and 26 are velocity vector fields taken at the tip (94% of the radius) at speeds of 16, 26, 32 m/s respectively for the straight blade. Values for the 20-Forward blade taken at the tip (94% of the radius) are illustrated in Figures 27, 28, and 29 at speeds of 16, 26, 32 m/s respectively. The 20-Forward blade has a larger trailing edge separation at the tip than the straight blade, which is also evident in plots of the pressure distribution, Figures 21-23. Even though there is more flow separation in the forward swept blades, the overall efficiency still surpasses that of the straight blade. Analysis of the velocity vector plots verifies the trend established by the C_p plots that the angle of attack of the swept blades decreases at a slower rate than the straight blade does.

There are three assumed reasons for the higher efficiency and larger stall margin for the swept blades:

First, the effective aspect ratio, AR_E, of the swept blades is slightly larger if AR_E is defined as:

$$AR_E = \frac{Leading\ \ Edge\ \ Length}{Maximum\ \ Blade\ \ Width} \tag{5.6}$$

This AR_E differs from the conventional AR for propellers by using the leading edge length in place of the blade radius. The straight, 10-15, and 20-Forward blades will produce effective aspect ratios of 3.962, 4.029, and 4.031 respectively. The AR_E of the 20-Forward blade is 1.7% larger than that of the straight. Such a slightly larger AR may help to reduce the induced drag and downwash.

Secondly, according to the swept wing theory, the velocity component normal to the leading edge is reduced. The swept blades in this research were designed to maintain identical chord lengths at the same radial locations as the straight blade. However, the chord length normal to the leading edge is shorter than that of the straight blade. These two factors contribute to reduce the profile drag of the airfoil.

Finally, similar to the flow of a compressor, it is speculated that an important factor is the 3D effect of the forward sweep, which pulls more mass flow in the tip region.[9] This causes the tip flow have more kinetic energy and suppresses the tip vortex. The weakened tip vortex will reduce the downwash and drag, thus maintaining an angle of attack closer to that desired over a wider range of freestream velocities. A detailed study of the tip vortices for the straight and swept blades will be conducted as research continues.

5. Future Studies

CFD simulations will be conducted for other designs in order to solidify the currently established trend. Wind tunnel tests which include the nacelle drag will be performed on the current blade designs. Also, new wind tunnel tests and CFD simulations with swept blades of a diameter closer to those used on full-size aircraft will be done to determine the effect of scaling. Finally, CFD simulations will be expanded in an effort to locate an optimal sweep angle and configuration, as well as to identify the 3D effects of forward swept blades that improve efficiency and stall margin.

6. Conclusions

This paper studied the performance of forward swept propeller blades by comparing them to a baseline straight blade. The forward sweep of all propellers was created by leaning the leading edge in the direction of rotation while remaining in the rotating plane. The projection of the leading edge on the axial-radial plane is a straight line with a constant axial position across the entire blade span. Hence, the blade has no sweep in the axial direction as described in the aerodynamic design method of this paper. Two forward swept blades, 10-15 backward-forward and 20-Forward, were studied in detail.

The preliminary wind tunnel tests show that the swept blades have higher efficiencies and larger stall margins than those of the straight blades. CFD simulations of the 3D propeller blades also confirm the same trend. The 20-Forward swept blade has the highest efficiencies and stall margin of all swept configurations studied. The CFD results show that the forward swept blades slow down the decreasing angle of attack and therefore have a larger range of the favorable angle of attack. At the same freestream velocities, the swept blade has a higher angle of attack and yields higher thrust and efficiency.

There are three suspected reasons why the swept blades have higher efficiencies and larger stall margins. First, the effective aspect ratio, as defined in this paper, is slightly larger. The AR of the 20-Forward is 1.7% larger than that of the straight blade. This slightly larger AR may help to reduce the induced drag and downwash. Secondly, according to the swept wing theory, the velocity component and chord length normal to the leading edge are reduced in the swept blades. These two factors contribute to reduce the profile drag of the airfoil. Finally, it is speculated that an important factor is the 3D effect created by the forward sweep, which pulls more mass flow in the tip region. This causes the tip flow to have more kinetic energy and suppresses the tip vortex. The weakened tip vortex will reduce the downwash and drag, thus maintaining an angle of attack closer to that desired over a wider range of freestream velocities.

Further wind tunnel tests will be conducted to exclude uncertainties related to the omission of the nacelle drag. Additional analysis of the CFD results will be conducted to fully understand the mechanism that causes the 3D effect of forward swept blades to improve efficiency and stall margin. An effort will be made, through CFD and wind tunnel tests, to determine the optimum sweep angle and configuration. Finally, new wind tunnel tests and CFD simulations will be carried out on full-size propellers to determine the effect of scaling.

7. Acknowledgements

We owe our deepest and most sincere thanks to the following companies, departments, and individuals for the assistance they rendered. Sermatech Castings, University of Miami, Department of Industrial Engineering, Hobby Lobby, DuPont, Florida International University, Stratasys International, Inc., University of Florida, Mr. Ryan Holman, Mr. Robert Jeracki at NASA Glenn Research Center, and the University of Miami, College of Engineering interdepartmental award issued to Dr. Ge-Cheng Zha (PI).

References

1. Whitcomb, Richard T. "A Discussion of the Design of Highly Swept Propeller Blades" – NACA RM L50A23. National Advisory Committee for Aeronautics, Washington; May 4, 1950.

2. R. J. Jeracki and G. A. Mitchell, "Low and High Speed Propellers for General Aviation-Performance Potential and Recent Wind Tunnel Test Results", NASA TM 81745, 1981.

3. R. J. Jeracki, D. C. Mikkelson, and B. J. Blaha, "Wind Tunnel Performance of Four Energy Efficient Propellers Design for Mach 0.8 Cruise", NASA TM 79124, 1979.

4. G. L. Stefko, and R. J. Jeracki, "Wind-Tunnel Results of Advanced High-Speed Propellers at Takeoff, Climb, and Landing Mach Numbers", NASA TM 87030, 1985.

5. C. J. Miller and J. P. Sullivan, "Noise Constraints Effecting Optimal Propeller Designs", NASA TM 86967, 1985.

6. D. C. Mikkelson and G. A. Mitchell, "Summery of Recent NASA Propeller Research", NASA TM 83733, 1984.

7. Nichols, G. H. "Design and Fabrication of Forward-Swept Counter-rotation Blade Configuration for Wind Tunnel Testing" – GE Advanced Technology Operations. Contract NAS3-25269, CR - 191193. March 1, 1994.

8. R. J. Jeracki, "Private Communication", NASA Glenn Research Center, April 2, 2002.

9. A.R. Wadia, P.N. Szucs, and D.W. CrallInner, "Inner Workings of aerodynamic Sweep", ASME Journal of Turbomachinery, Vol. 120, Oct. 1998.

10. G. C. Zha, "Arched Wings: Possible Improvement of the Wing Performance", AIAA Paper-94-0054, 1994.

11. Freeman, Hugh B. *Comparisons of Full-Scale Propellers Having R.A.F.-6 and Clark Y Airfoil Sections*; Langley Memorial Aeronautical Laboratory, NACA; Oct. 8, 1930.

12. Weick, Fred E. *Aircraft Propeller Design*. McGraw-Hill Book Company, Inc. New York; 1930.

13. Barlow, Jewel B., Alan Pope, and William H. Rae, Jr. *Low Speed Wind Tunnel Testing 3rd Edition*. John Wiley & Sons, Inc., New York; 1999, pg. 509, 534-536.

14. *Fluent 6.0 User's Guide*, Fluent Incorporated, 2002.

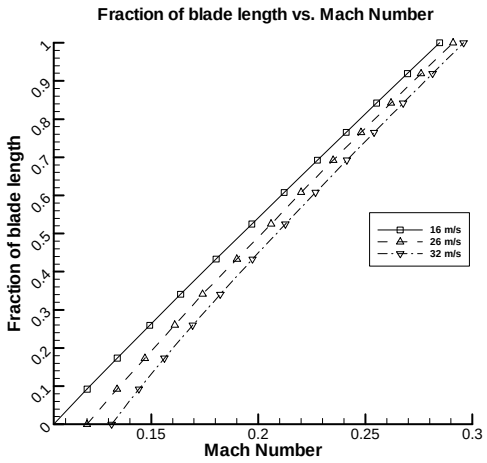

Figure 1: Mach number along the blade at different speeds

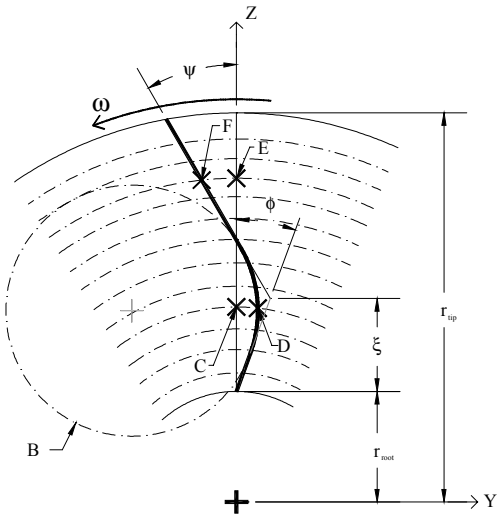

Figure 2: Combined backward-forward swept design configuration

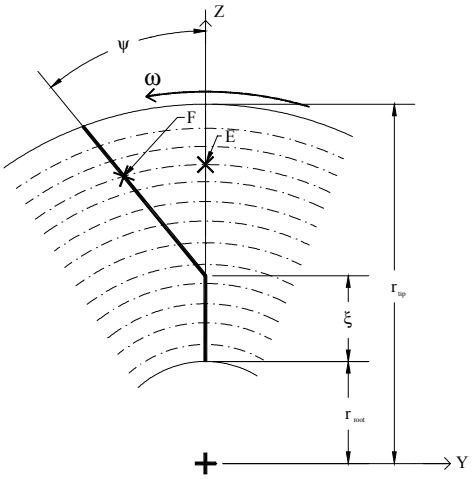

Figure 3: Delayed forward sweep design configuration

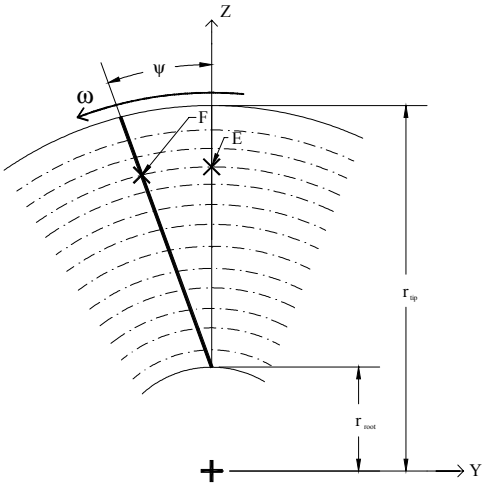

Figure 4: Completely forward swept design configuration

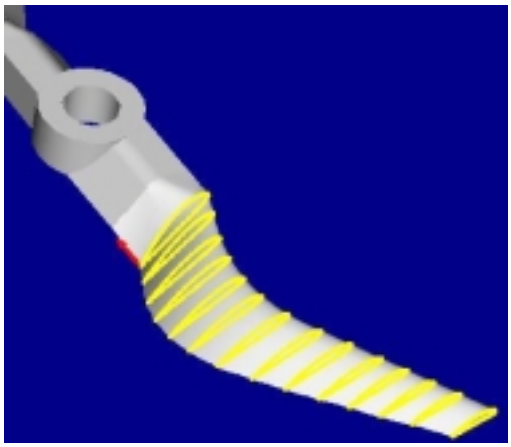

Figure 5: Stacking of the airfoil for a swept blade

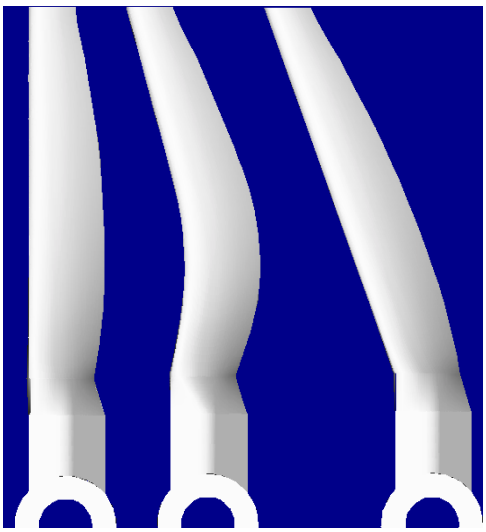

Figure 6: Pro/E propeller geometry

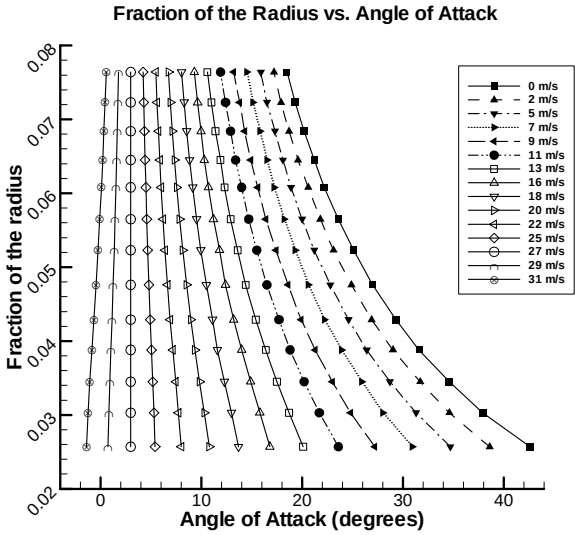

Figure 7: Fraction of the radius vs. angle of attack for select velocities

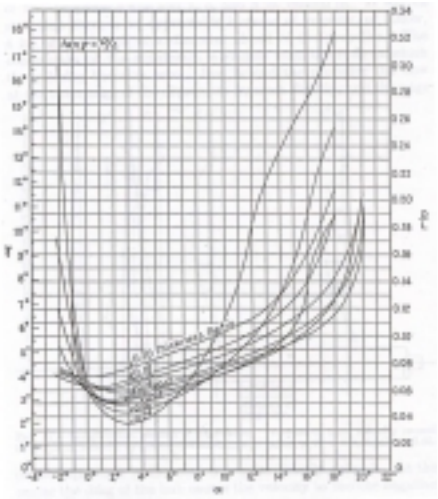

Figure 8: R.A.F.-6 D/L vs. angle of attack[12]

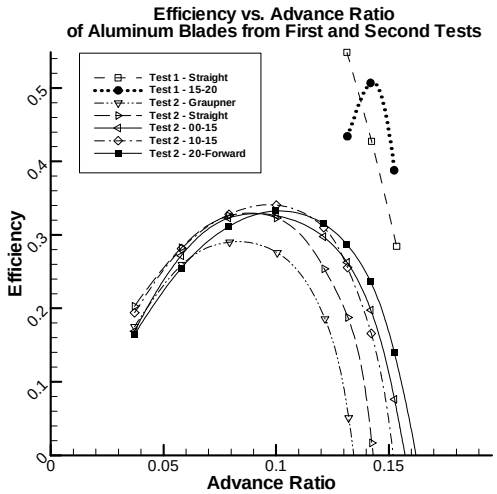

Figure 9: Wind tunnel efficiency vs. advance ratio results

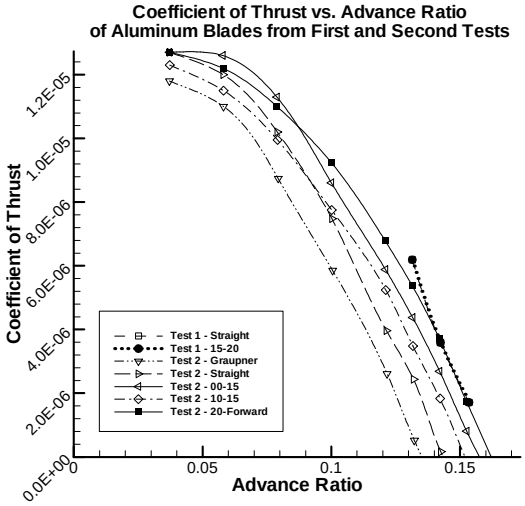

Figure 10: Coefficient of thrust for wind tunnel tests

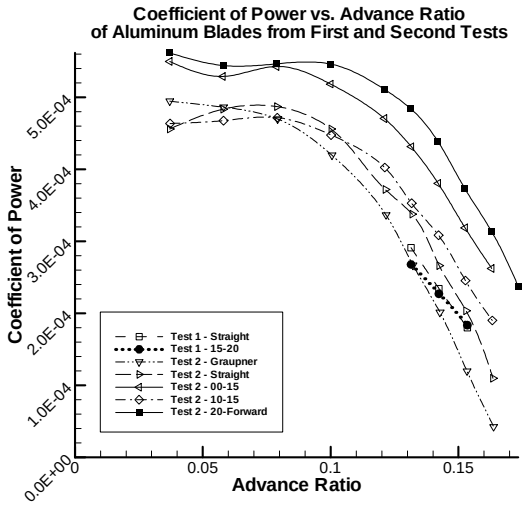

Figure 11: Coefficient of power for wind tunnel tests

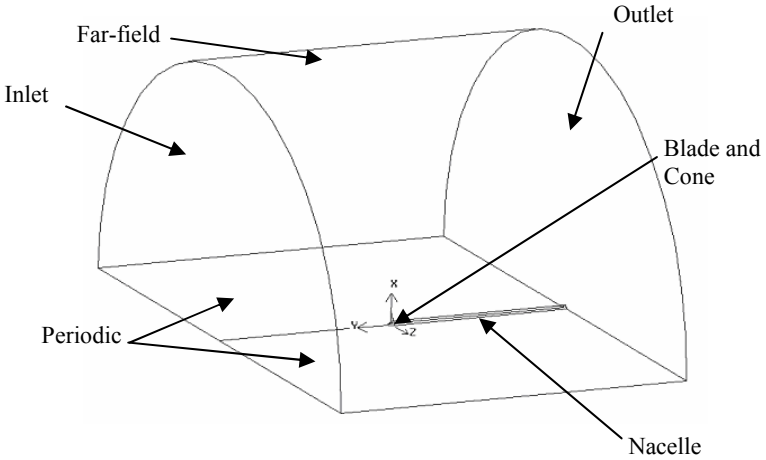

Figure 12: Isometric view of the CFD flow regime

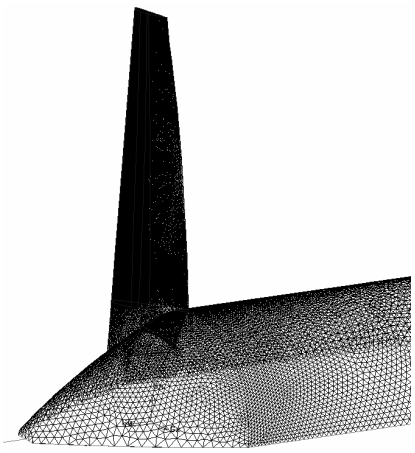

Figure 13: Isometric view of blade, cone, and nacelle

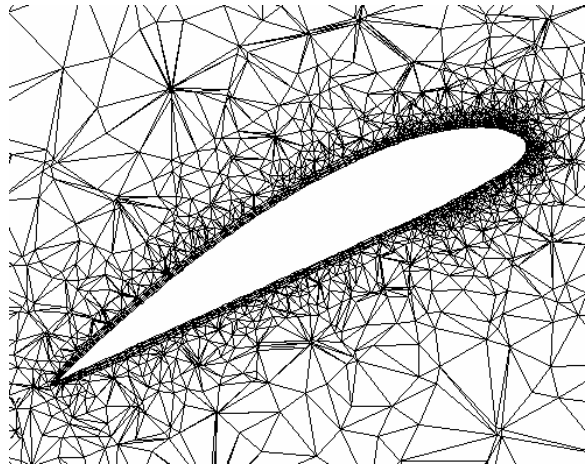

Figure 14: Mid-blade flow regime volume mesh

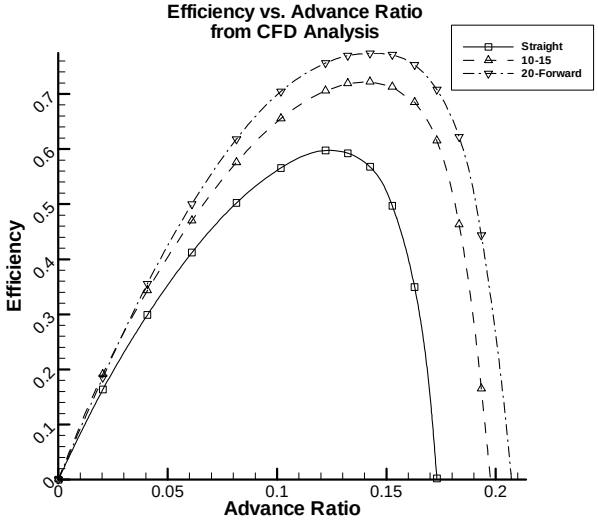

Figure 15: Efficiency vs. Advance ratio from CFD results

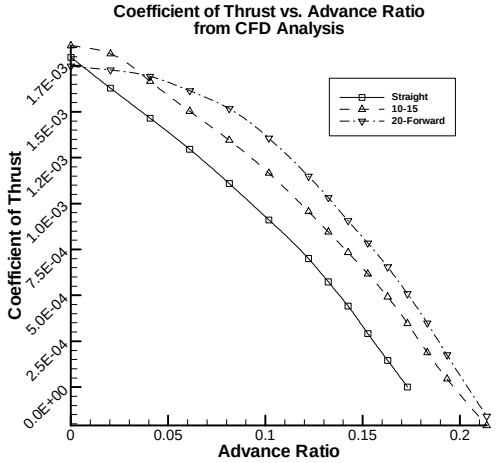

Figure 16: Coefficient of Thrust vs. Advance Ratio from CFD results.

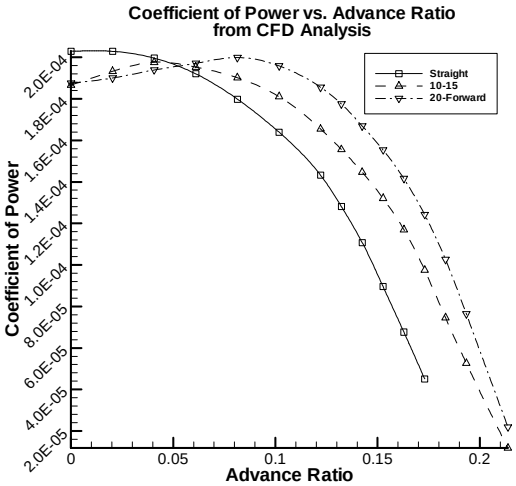

Figure 17: Coefficient of Power vs. Advance Ratio from CFD Results.

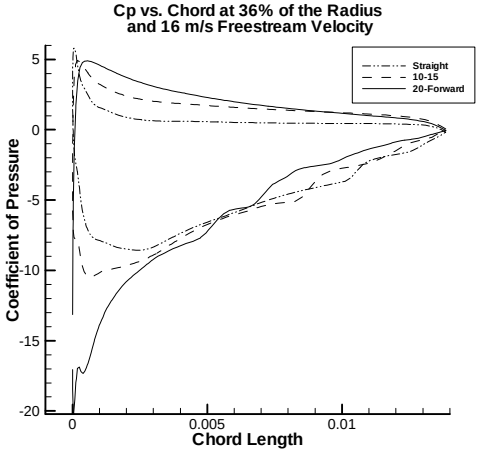

Figure 18: CP vs. Chord length located at 36% of the blade radius with a freestream velocity of 16 m/s

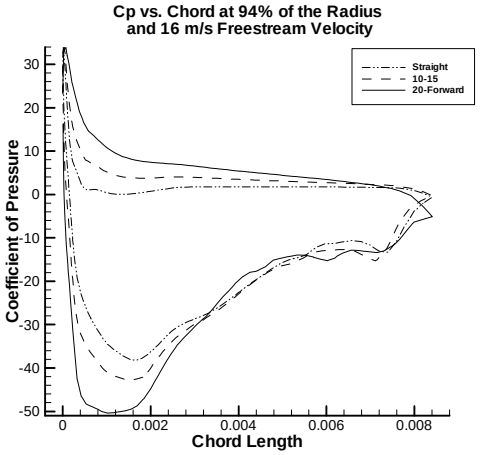

Figure 21: CP vs. Chord length located at 94% of the blade radius with a freestream velocity of 16 m/s

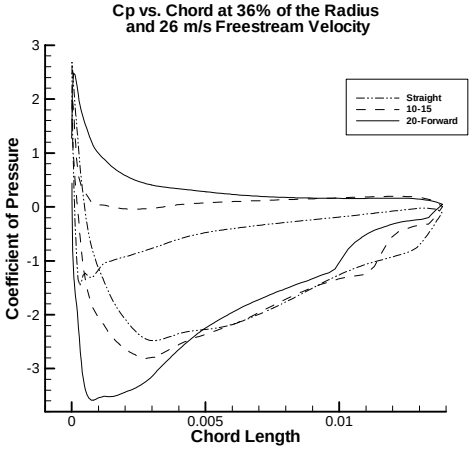

Figure 19: CP vs. Chord length located at 36% of the blade radius with a freestream velocity of 26 m/s

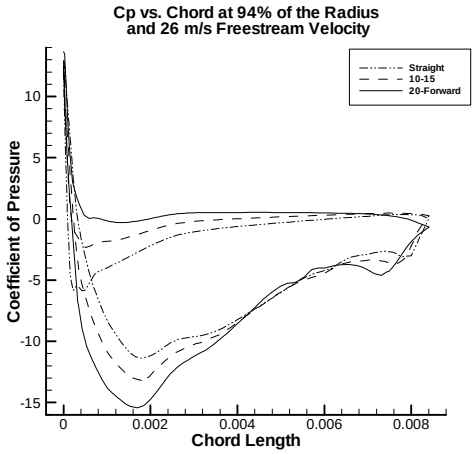

Figure 22: CP vs. Chord length located at 94% of the blade radius with a freestream velocity of 26 m/s

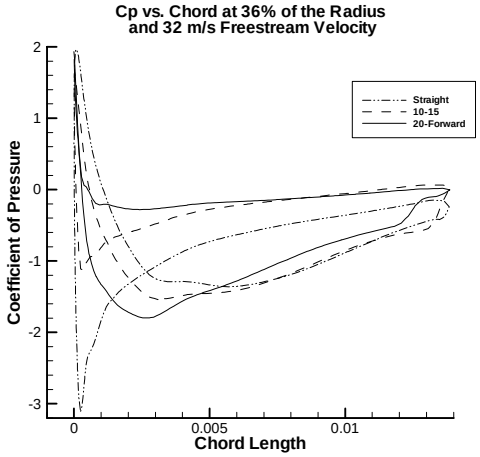

Figure 20: CP vs. Chord length located at 36% of the blade radius with a freestream velocity of 32 m/s

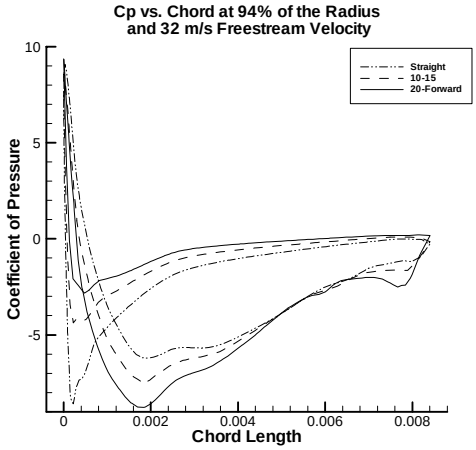

Figure 23: CP vs. Chord length located at 94% of the blade radius with a freestream velocity of 32 m/s

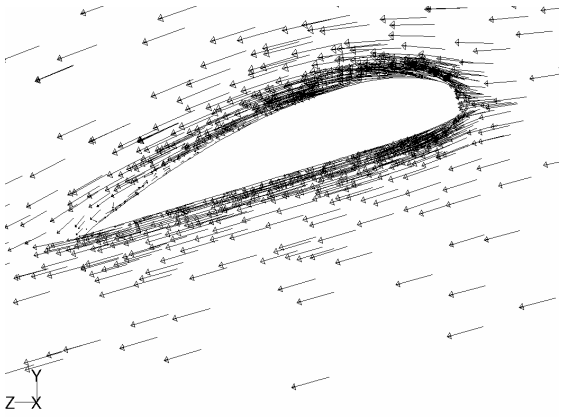

Figure 24: CFD Vector field for the straight propeller at 16 m/s at 94% of the blade radius

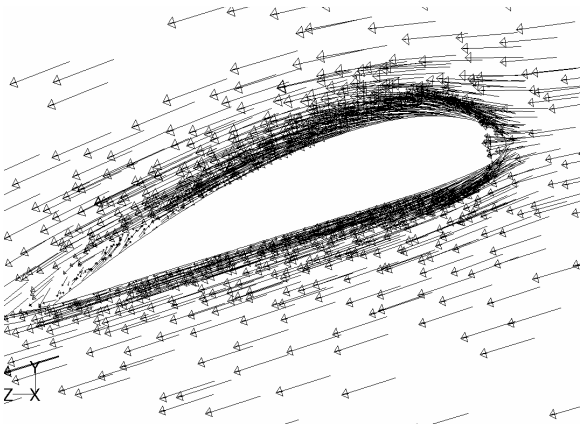

Figure 27: CFD Vector field for the 20-Forward propeller at 16 m/s at 94% of the blade radius

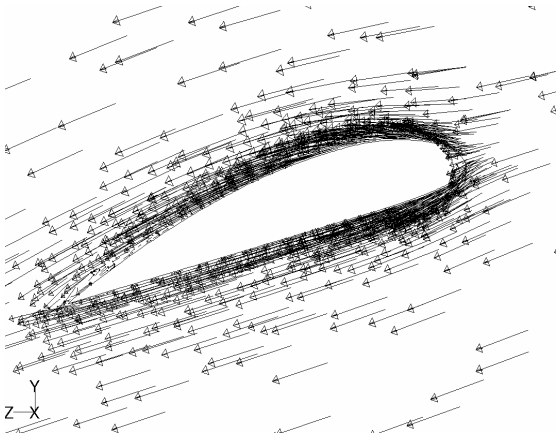

Figure 25: CFD Vector field for the straight propeller at 26 m/s at 94% of the blade radius

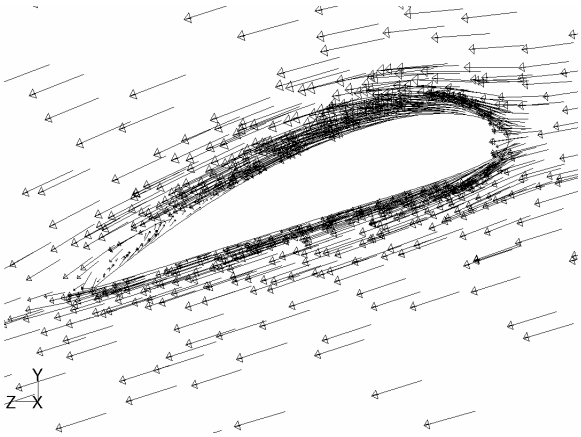

Figure 28: CFD Vector field for the 20-Forward propeller at 26 m/s at 94% of the blade radius

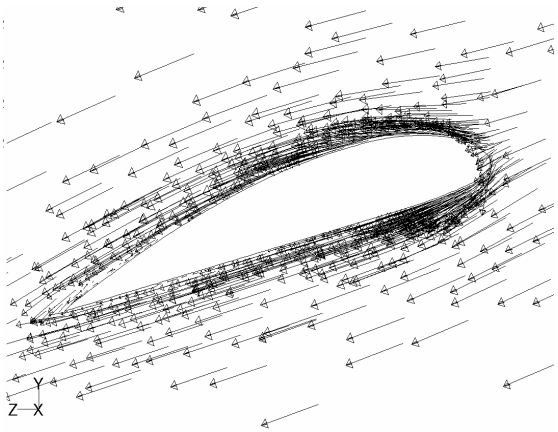

Figure 26: CFD Vector field for the straight propeller at 32 m/s at 94% of the blade radius

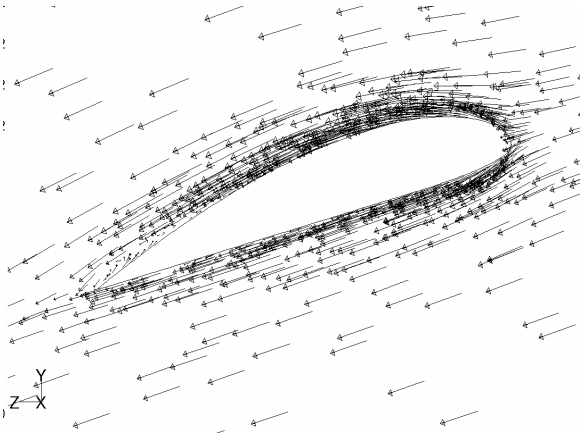

Figure 29: CFD Vector field for the 20-Forward propeller at 32 m/s at 94% of the blade radius